ADVANCED FUNCTIONAL MATERIALS
www.afm-journal.de

HtrA3-Mediated Endothelial Cell–Extracellular Matrix Crosstalk Regulates Tip Cell Specification

Yaru Guo, Siqin Ma, Mingming Xu, Yan Wei, Xuehui Zhang, Ying Huang, Ying He, Boon Chin Heng, Lili Chen, and Xuliang Deng**

Angiogenesis is critical in tissue engineering and regenerative medicine. Once initiated, outgrowing capillaries are spearheaded by specialized endothelial cells (ECs) termed tip cells. Specification of tip cells from ECs during angiogenesis is greatly influenced by the surrounding extracellular matrix (ECM). However, the crosstalk between ECs and the ECM in tip cell specification is poorly understood. Here, this study shows that the high-temperature requirement A3 (HtrA3) protein is deeply involved in this process. Specifically, HtrA3 is upregulated in the frontal area of tissue repair and cancer progression through VEGFR2 activation by VEGF in ECs. Secreted HtrA3 degrades the surrounding Collagen IV, which provides space for tip cell morphogenesis and exposes integrin β1-related ligands. Integrin β1-ligand binding activates PI3K/AKT/mTOR signaling, which subsequently suppresses the Notch signaling pathway, eventually promoting tip cell specification. Moreover, local administration of exogeneous recombinant HtrA3 in rat cranial bone defects significantly increases blood vessel formation. Conversely, injection of HtrA3 siRNA decreases developmental retinal angiogenesis. These data show that HtrA3 mediated crosstalk between ECs and the ECM enhances tip cell specification of ECs. Hence, HtrA3 can act as a therapeutic agent for improving angiogenesis in situations in need, as well as serve as a therapeutic target for pathological angiogenesis.

1. Introduction

Angiogenesis is a highly coordinated process and is essential in many physiological and pathological processes, including embryo development, tumorigenesis, tissue engineering and regenerative medicine.[1] Generally, angiogenesis is initiated from the preexisting vasculature by sprouting of endothelial cells (ECs). Once initiated, outgrowing capillaries are spearheaded by specialized ECs termed tip cells, which are followed by stalk cells.[2] Tip cells are characterized by long and dynamic filopodia, which they use to probe the environment for directional cues.[3] Moreover, anastomosis of tip cell filopodia leads to the formation of new vessel branches and excessive tip cells will lead to hyperbranched vascular networks.[4] Therefore, the specification of endothelial tip and stalk cells is a major control point in angiogenesis.[5] Previous studies have showed that formation of tip cells is prominently regulated by Notch signaling.[6] However, as shown in **Figure 1**A, tip cell selection in vivo is a dynamic process. Cellular state is not unchangeable and subtypes of endothelial cells can overtake each other to compete for the tip position in a sprout, a phenomenon termed tip cell overtaking.[7] Cell competition is imminent in the selection of a leading tip during angiogenesis. Therefore, the precise mechanisms regulating this process might be more complex than Notch signal alone and thus remain to be determined.

ECs are surrounded by a complex extracellular matrix (ECM), which serves not only as a key scaffolding material but also as

Dr. Y. Guo, Dr. S. Ma, Dr. M. Xu, Prof. Y. Wei, Dr. Y. Huang, Dr. Y. He, Prof. X. Deng
Beijing Laboratory of Biomedical Materials
Department of Geriatric Dentistry
Peking University School and Hospital of Stomatology
Beijing 100081, P. R. China
E-mail: kqdengxuliang@bjmu.edu.cn

Prof. X. Zhang
Department of Dental Materials & Dental Medical Devices Testing Center
National Engineering Laboratory for Digital and Material Technology of Stomatology
Peking University School and Hospital of Stomatology
Beijing 100081, P. R. China

Prof. B. C. Heng
Central Laboratory
Peking University School and Hospital of Stomatology
Beijing 100081, P. R. China

Prof. L. Chen
Department of Stomatology
Union Hospital
Tongji Medical College
Huazhong University of Science and Technology
Wuhan 430022, China
E-mail: chenlili1030@hust.edu.cn

Prof. L. Chen
Hubei Province Key Laboratory of Oral and Maxillofacial Development and Regeneration
Wuhan 430022, China

The ORCID identification number(s) for the author(s) of this article can be found under https://doi.org/10.1002/adfm.202100633.

DOI: 10.1002/adfm.202100633

 © 2021 Wiley-VCH GmbH

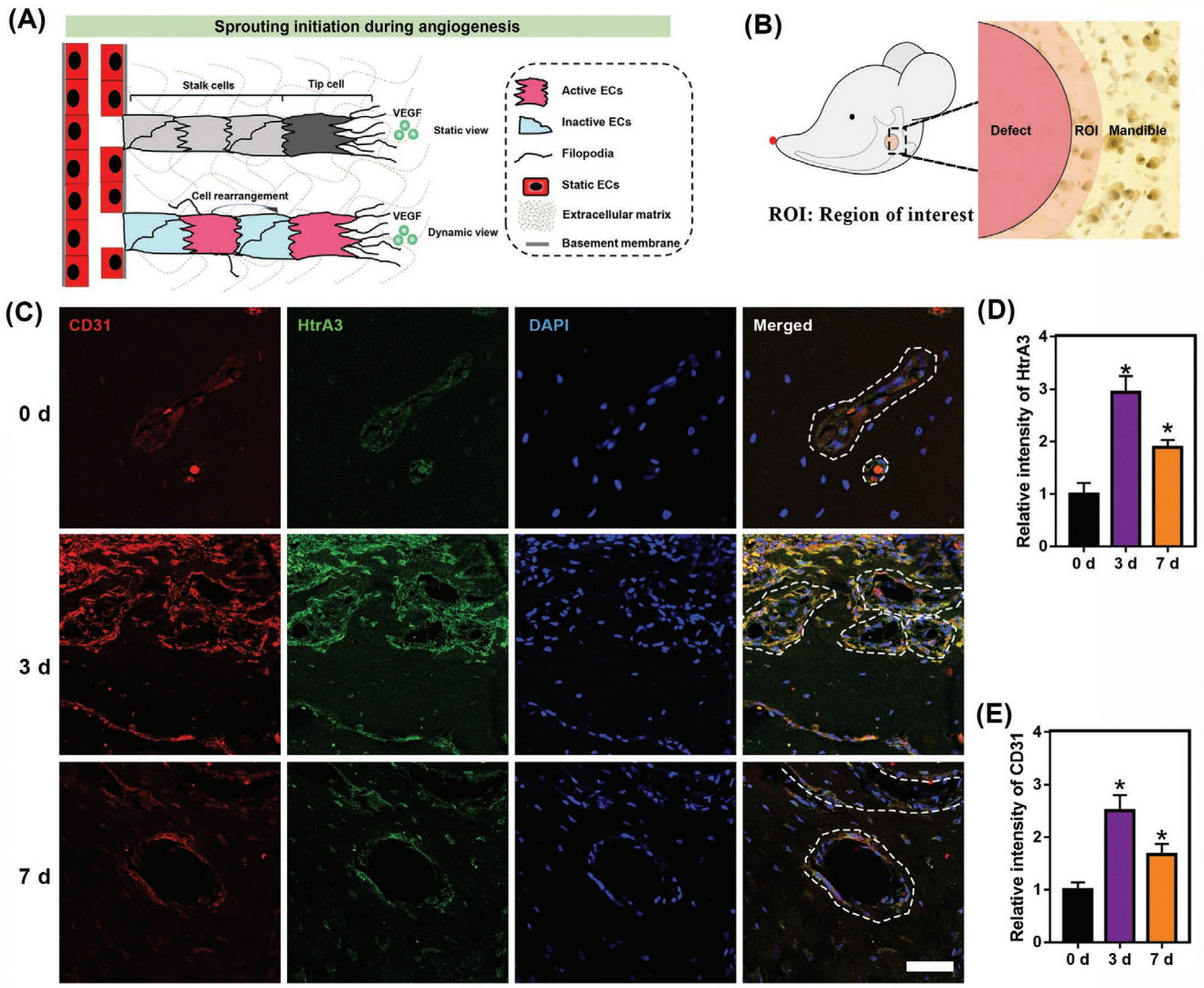

Figure 1. HtrA3 was upregulated in ECs under some physiological and pathological conditions A) Schematic of a sprout showing the differential properties of its ECs. In a dynamic view, ECs can overtake each other to compete for the tip (cell rearrangement and tip cell overtaking). B) Model of bone defect on rat mandible and the region of interest (ROI). C) Immunofluorescent staining results of ROI showed that HtrA3 was upregulated in ECs at the front of bone defect repair from day 0 to day 3, which decreased on day 7. (Dotted lines mark blood vessels, scale bar: 50 µm). D) Quantification analysis of relative HtrA3 intensity on 0, 3, 7 days. E) Quantification analysis of relative CD31 intensity on 0, 3, 7 days. (*$p < 0.05$).

a physical barrier for new vessel formation. The position of tip cells determines its distinct ECM microenvironment from stalk cells. Presumably, EC-ECM interaction should play an essential role in the dynamic competition process of tip cell selection. The crosstalk between ECs and ECM is ubiquitous during sprouting angiogenesis. Specifically, ECs secrete proteinases to remodel the ECM, originating with breakdown of the basement membrane (BM) to allow for EC breakthrough, migration, and proliferation. In return, ECM remodeling can release both anti-angiogenic proteolytic fragments and pro-angiogenic growth factors that would remain otherwise bound to the ECM.[8] Previous studies have showed multiple matrix metalloproteinases (MMPs), including MMP-1, MMP-2, MMP-8, MMP-13 and MMP-14, and display type I collagenolytic activities.[9] However, BM, which is the first to be degraded with angiogenesis initiation, are thought to contain predominantly the collagen type IV. Although gelatinases (MMP-9 and MMP-2) have been reported to degrade type IV of collagen, they are predominantly produced by stromal and immune cells.[10] Therefore, it is imperative to know if other proteinases are EC-autonomously involved in the EC-ECM interaction, reducing physical barrier for initiation of new vessel formation, providing the space for tip cell morphogenesis, and, may be more importantly, participating in selecting the most competitive ECs to be tip cells during angiogenesis.

HtrA3 is a member of the high-temperature requirement A (HtrA) family of serine proteases, which is well conserved in evolution. It is originally identified as a pregnancy-associated serine protease due to its up-regulation in the placenta.[11] Since then, HtrA3 has been shown involved in many physiological and pathological processes, including embryo implantation, bone defect repair, inflammation, and oncogenesis.[12] However,

© 2021 Wiley-VCH GmbH

the precise mechanism by which HtrA3 is involved in these processes remains to be determined. Since angiogenesis is a fundamental element in the aforementioned situations where HtrA3 is upregulated, further research on the role of HtrA3 in angiogenesis might help to deepen our understanding of the function of HtrA3 and the mechanism of angiogenesis. Here, by using loss of function (LOF) and gain of function (GOF), we find that HtrA3 promotes angiogenic sprouting and tip cell formation through mediating EC-ECM interaction. We identify that suppression of Notch signaling contributes to the enhanced sprouting capacity of ECs with HtrA3 upregulation. Moreover, through HtrA3 administration, angiogenesis in defect area is achieved. Together, these results reveal that HtrA3 is a critical regulator of ECs governing angiogenic sprouting and implicate a therapeutic application of HtrA3 in regulating angiogenesis.

2. Results and Discussion

2.1. HtrA3 is Highly Expressed in the Frontal Area of Tissue Repair and Tumor Invasion

We investigated HtrA3 expression under certain physiological and pathological conditions. First, we created full-thickness defects in rat mandibles and detected the expression of HtrA3 at the edge of the defect on day 0, day 3, and day 7 post-operation respectively (Figure 1B). The immunofluorescence staining results showed that the expression of HtrA3 was barely detected in ECs near the defect border immediately after the operation (day 0). It peaked on day 3 and then declined considerably till day 7 (Figure 1C,D). Similarly, we created skin wounds in mice (Figure S1A, Supporting Information) and found that, on day 4 post-operation, HtrA3 was highly expressed in ECs within the frontal areas of skin wounds, rather than those far from the margin of wounds (Figure S1C,E, Supporting Information). Furthermore, we observed a higher HtrA3 expression level in ECs in oral squamous cell carcinoma (OSCC) tissues, compared with that in normal adjacent tissues (Figure S1B,D,F, Supporting Information).

Interestingly, CD31, a maker of ECs, was highly expressed at the edge of mandibular defects, skin wounds, and tumor invasion (Figure 1E; Figure S1E,F, Supporting Information), which coincided with the expression of HtrA3. These findings indicate that HtrA3 expression is closely associated with neovascularization. In addition, previous studies have reported that HtrA3 is highly expressed during embryo implantation, inflammation, and oncogenesis,[12a,b] processes that are closely correlated with strong demand for blood supply and rich blood vessels. Hence, we hypothesize that HtrA3 is deeply implicated in angiogenesis within many physiological and pathological processes.

2.2. HtrA3 Upregulation in hUVECs Promotes Tube Formation In Vitro and Subcutaneous Angiogenesis in Nude Mice

We next explored whether HtrA3 can enhance angiogenesis of ECs in vitro and in vivo. Here, human umbilical vein ECs (hUVECs) are utilized as an EC model to explore the roles of HtrA3 in ECs function. We transfected HUVECs with lentivirus to overexpress or knock down the HtrA3 gene (Figure S2, Supporting Information). We found that HtrA3 was present in conditioned media, confirming it's secretory characteristics (Figure S2C, Supporting Information). Though tube formation assay, we observed that the total tubule length, number of junctions and tubules are significantly increased in HtrA3-overexpressed hUVECs (**Figure 2**A,C). Then, hUVECs embedded in matrigel were injected subcutaneously into nude mice to explore the effect of HtrA3 on angiogenesis in vivo. After 4 days transplantation, we found that the HtrA3-overexpressed hUVECs group displayed 1.5-fold more capillary interconnections, 2-fold more vascular tubules and 5-fold greater blood vessel area per unit area than the vehicle control group (Figure 2B,D). Moreover, we observed new sprouts from the present blood vessels in the HtrA3-overexpressed group (white arrow in Figure 2B). On the contrary, smaller blood vessels with less capillary interconnections and decreased total cross-sectional area were observed in the HtrA3-knockdown group (Figure S3A,B, Supporting Information). These data showed that HtrA3 upregulation in hUVECs promotes tube formation in vitro and subcutaneous blood vessel regeneration in vivo, thereby indicating that HtrA3 promotes angiogenesis of endothelial cells.

2.3. HtrA3 Enhances Sprouting, Cellular Cortical Protrusions, and Mobility of hUVECs

Having established the crucial role of HtrA3 in angiogenesis, we then explored the roles of HtrA3 in regulating various functions of hUVECs including sprouting, cellular shape, mobility, and proliferation. To determine whether HtrA3 regulates hUVECs sprouting, spheroid-based angiogenesis assay was adopted. We found that HtrA3-overexpressing hUVECs spheroids exhibited larger numbers of sprouts and increased invasion distance into the matrix (Figure 2E,F) while HtrA3-knockdown hUVECs spheroids exhibited less extensions and decreased invasion distance into the matrix (Figure S4A, Supporting Information). Treatment of HtrA3-knockdown spheroids with exogenous recombinant human HtrA3 (rhHtrA3) restored invasion distance and extensions (Figure S4B–E, Supporting Information), indicating that HtrA3 enhanced hUVEC sprouting.

We also observed that HtrA3-overexpressing hUVECs exhibited more cellular filopodial protrusions (Figure 2G) which are critical for tip cells to sprout, migrate, and sense guidance cues provided by soluble, cell, or matrix-bound factors.[3] Cellular sphericity and volume were used as parameters to quantify cellular shape variation. We found that HtrA3 overexpression in hUVECs significantly decreased cellular sphericity and increased their volume (Figure 2H), whereas HtrA3-knockdown hUVECs displayed completely smooth sphericity and decreased volume (Figure S4F, Supporting Information). Addition of rhHtrA3 to the HtrA3-knockdown group restored the cortical protrusions and cellular volume (Figure S4G–J, Supporting Information), indicating that HtrA3 increases cellular cortical protrusions of hUVECs extending into the surrounding Matrigel.

Subsequently, the motility of HUVECs was assessed by transwell cell invasion assessment and wound healing assay. In the

© 2021 Wiley-VCH GmbH

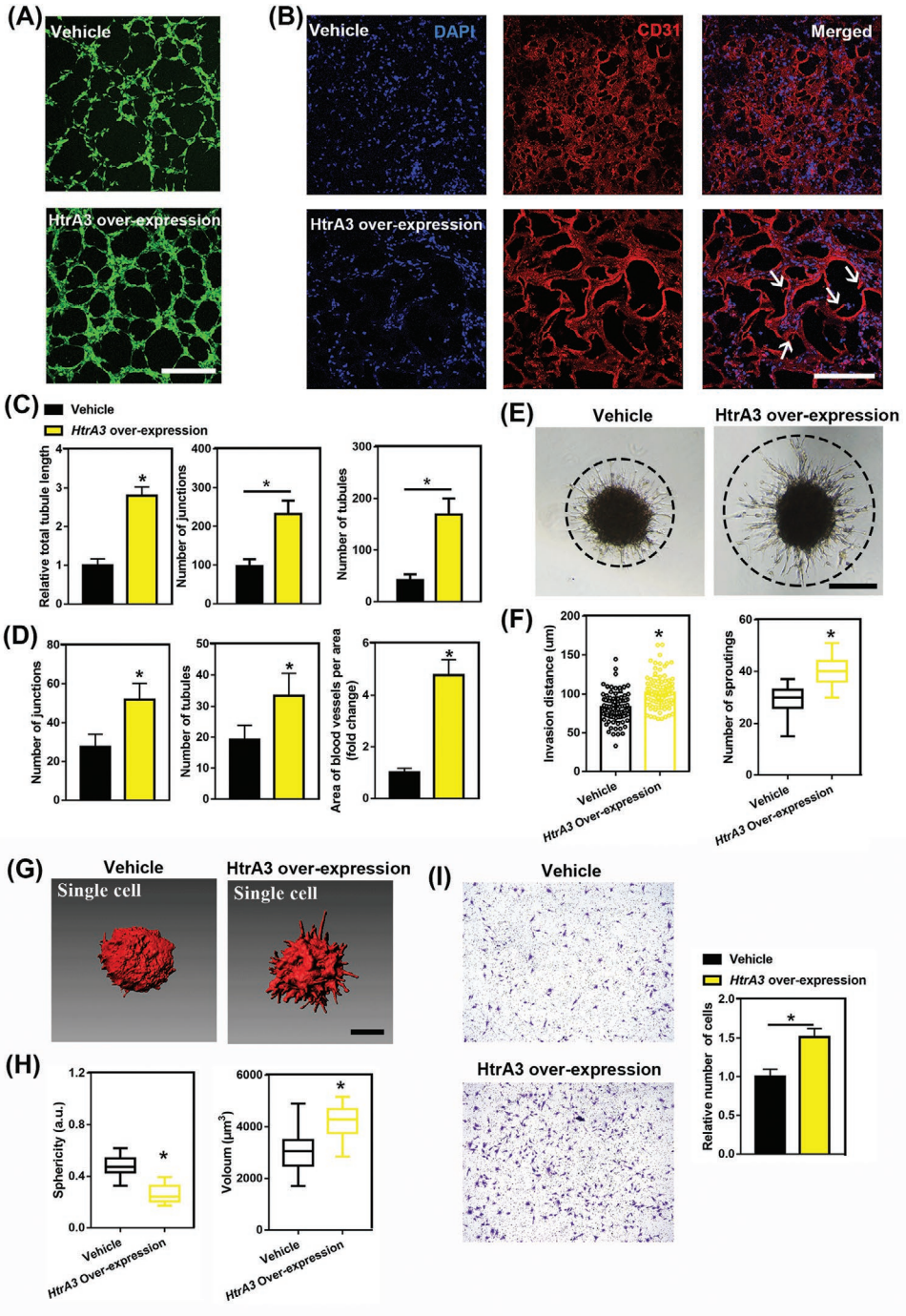

Figure 2. HtrA3 promoted angiogenesis in vitro and in vivo and enhanced functions of hUVECs, including sprouting, cellular F-actin-positive protrusions, and mobility. A) Representative images of tube formation at 6 h after cells were seeded on Matrigel (Scale bar: 500 μm), showing increased relative total tube length, number of junctions, and number of tubules after HtrA3 overexpression, as shown in (C). B) Confocal immunofluorescence images of subcutaneous transplantation of hUVECs transfected with vehicle or HtrA3 over-expressing lentiviral vectors in nude mice for 4 days. (Scale bar: 200 μm), indicating that HtrA3 increased the number of junctions, number of tubules, and area of blood vessels as shown in (D). E) The representative photomicrographs of 3D in vitro sprouting angiogenesis showed that HtrA3 enhanced angiogenesis, exhibiting higher cellular invasion distance and more sprouts into matrices (F). (Scale bar: 200 μm) G) Representative microscopy images of hUVECs cultured in matrices for 24 h (single cell), visualized by F-actin-positive pixel reconstruction, indicating that HtrA3 promoted cortical protrusions into matrices. (Scale bar: 10 μm). H) Quantification analysis of sphericity and volume of different hUVECs, indicating that HtrA3 significantly decreased the sphericity and enhanced the volume. I) The representative photomicrographs of different ECs in the transwell cell invasion assay showed that HtrA3 promoted the invasion of hUVECs. The quantification analysis of the number of hUVECs invasion across the membrane are shown on the right. (*$p < 0.05$).

 © 2021 Wiley-VCH GmbH

transwell cell invasion assay, we observed that the number of hUVECs from the upper chamber across the membrane were significantly increased in the HtrA3-overexpression group (Figure 2I), while less cells across the membrane were observed in the HtrA3-knockdown group (Figure S5A, Supporting Information). In the wound healing assay, we observed that HtrA3-overexpressing hUVECs migrated closer toward the middle of the wound (Figure S5B, Supporting Information). The HtrA3-knockdown group resulted in less reduction in the wound area (Figure S5B, Supporting Information). Addition of rhHtrA3 to the HtrA3-knockdown group reversed wound areas in the wound healing assay (Figure S5C, Supporting Information). Meanwhile, higher HtrA3 expression was observed in cells at the front of the migration (Figure S5D, Supporting Information), thus indicating that HtrA3 promotes hUVECs mobility. However, we found that HtrA3 exerted negligible effects on the proliferation of hUVECs through real-time observation (Figure S5E, Supporting Information) and EdU (Figure S5F, Supporting Information) assays.

During the angiogenic process, quiescent endothelial cells are first activated and differentiated into two alternative fates: tip cells or stalk cells. Tip cells are characterized by enhanced migratory propensity, extension of filopodia, without increased proliferation.[13] As mentioned earlier, the characteristics of HtrA3-overexpressing hUVECs are consistent with those of tip cells, and we therefore inferred that HtrA3 might contribute to tip cell formation.

2.4. HtrA3 Enhanced hUVECs Tip Cell Formation and Tip Position Competition

To validate our inference, we investigated the effects of HtrA3 on tip cell formation by hUVECs. We selected the cell membrane protein CD34 to mark tip cells in hUVEC cultures.[13] We found that HtrA3 expression in $CD34^+$ hUVECs was twice that of $CD34^-$ hUVECs (**Figure 3**A), indicating higher HtrA3 expression in tip cells. With flow cytometry, we found a higher percentage of $CD34^+$ cells among HtrA3-overexpressing hUVECs (Figure 3B). In the HtrA3-knockdown group, the proportion of $CD34^+$ cells declined dramatically (Figure S6A, Supporting Information). We next found that mRNA levels of tip cell-enriched gene transcripts, indicating CD34, VEGFR-2, CXCR4, and EFNB2,[13,14] increased in HtrA3-overexpressing hUVECs (Figure 3C) while it decreased significantly in HtrA3-knockdown hUVECs (Figure S6B, Supporting Information). The corresponding protein expression levels were also increased in HtrA3-overexpressing hUVECs (Figure 3D), but decreased in HtrA3-knockdown hUVECs (Figure S6C, Supporting Information). Moreover, HtrA3-overexpressing $CD34^+$ hUVECs exhibited greater numbers of longer filopodia (Figure 3E,G) while fewer and shorter filopodia were observed in HtrA3-knockdown hUVECs (Figure S6D, Supporting Information). Upon exposure to rhHtrA3, the inhibitory effects of HtrA3 knockdown on the proportion of $CD34^+$ cells were abrogated (Figure S7A, Supporting Information). These tip cell-enriched proteins (Figure S7B,C, Supporting Information) and and filopodia (Figure S7D, Supporting Information) in HtrA3-knockdown hUVECs were restored. Thus, all these data indicate that HtrA3 enhances tip cell specification of hUVECs.

During angiogenesis, ECs compete for the tip position through tip cell overtaking.[7a,b] Only the most competitive ECs occupying the tip position and leading the sprout can become tip cells. Then, we performed the mosaic spheroid assay to explore if HtrA3 improved hUVECs competition for the tip positions. Specifically, lentiviral vectors encoding the green fluorescent protein (GFP) gene were transfected to achieve $hUVECs^{GFP}$. Lentiviral vectors encoding both HtrA3 and GFP genes were transfected to achieve $hUVECs^{HtrA3;\ GFP}$. Vectors encoding the mCherry gene (displaying red fluorescence under confocal microscopy) were transfected to achieve $hUVECs^{RED}$. Two types of mosaic spheroids of $hUVECs^{GFP}/hUVECs^{RED}$ and $hUVECs^{HtrA3;GFP}/hUVECs^{RED}$ were constructed, with the two component cell populations mixed 1:1. After 24 h culture, the color at the tip area of sprouts from the spheroids was counted to quantify the contribution of $hUVECs^{HtrA3;GFP}$, $hUVECs^{GFP}$ or $hUVECs^{RED}$ to tip positions. We found that in spheroids of $hUVECs^{GFP}/hUVECs^{RED}$, stained green and red respectively contributed to 48.3% and 51.7% of the tip positions, indicating that $hUVECs^{GFP}$ was as competitive as $hUVECs^{RED}$ for the tip positions (Figure 3F,H,I). By contrast, in spheroids of $hUVECs^{HtrA3;GFP}/hUVECs^{RED}$, green staining contributed to 71.4% of the tip position (Figure 3F,H,I), indicating that $hUVECs^{HtrA3;GFP}$ was more competitive for tip positions. Therefore, we infer that HtrA3 enhances the likelihood of hUVECs occupying the tip area of angiogenic sprouts.

2.5. HtrA3 Promotes Tip Cell Formation Via the Itgβ1-PI3K/AKT/mTOR-Notch Signaling Axis

We then explored how HtrA3 promoted ECs tip cell specification. The tip cell selection is controlled by Notch signaling through lateral inhibition.[6] Inhibition of Notch signaling contributes to excessive tip cell formation, dramatically augmenting sprouting, branching, and hyperfusion of developing vessels in vivo. Since the observed hyperbranching and increase in angiogenic cell behavior and migration after HtrA3 over-expression are reminiscent of the effects of loss of Notch signaling, we next investigated whether HtrA3 promotes the angiogenic phenotype and tip cell formation in ECs by modulation of Notch signaling. We found that Notch-intracellular domain (NICD) and the mRNA expression levels of Notch target genes (Hey1, Hey2, HeyL, Hes1, and Hes2)[15] decreased in HtrA3-overexpressing hUVECs (**Figure 4**A,B). In HtrA3-knockdown hUVECs, these were apparently increased (Figure S8A,B, Supporting Information). Moreover, exposure of HtrA3-knockdown hUVECs to exogenous rhHtrA3 abrogated the increased NICD and Notch target genes expression levels (Figure S8C and D, Supporting Information). We activated Notch signaling with recombinant human DLL4 (rhDLL4) in HtrA3-overexpressing hUVECs, and found that the sprouting (Figure 4C,D) and tip cell markers (Figure 4E), including CD34, VEGFR2, CXCR4 and EphrinB2, decreased to levels similar to control hUVECs. When the Notch signaling pathway was inhibited with DAPT in *HtrA3*-knockdown hUVECs, sprouting number and invasion distance were apparently increased (Figure S8E and F,

 © 2021 Wiley-VCH GmbH

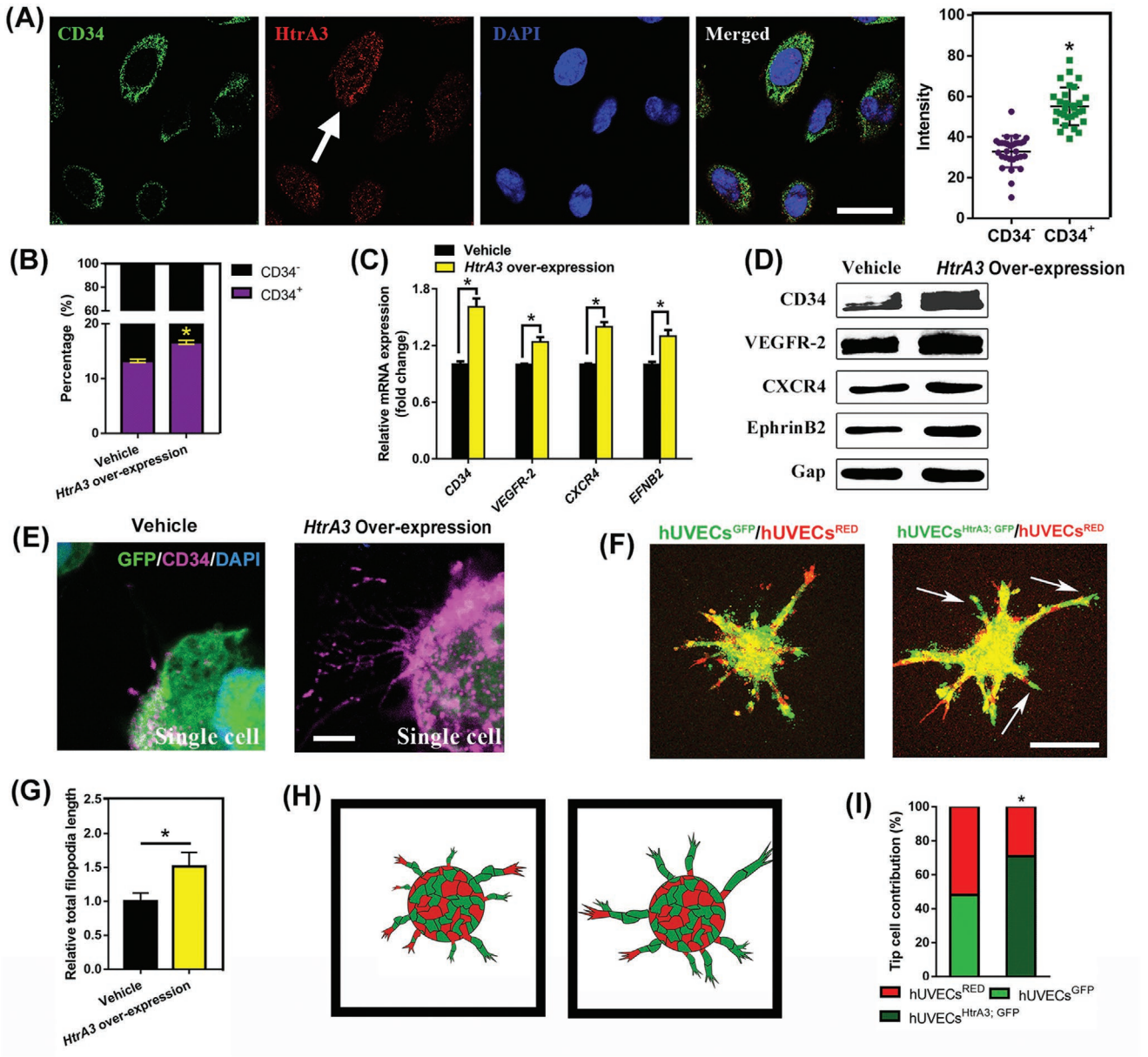

Figure 3. HtrA3 enhanced tip cell formation. A) HtrA3 (white arrow) was upregulated in CD34⁺ cells (tip cells). (Scale bar: 15 µm) B) Flow cytometry indicated that the percentage of CD34⁺ cells was upregulated by HtrA3. C) qPCR and D) Western blot analysis showed that HtrA3 promoted expression of tip cell markers both at the mRNA (including CD34, VEGFR-2, CXCR4 and EFNB2) and protein levels (including CD34, VEGFR-2, CXCR4, and EphrinB2). E) HtrA3 over-expression led to increased number and length of filopodia on tip cells (single cell, Scale bar: 5 µm), with the quantitative analysis of filopodia of tip cells being shown in (G). F) Representative images of EC mosaic spheroids for 1:1 $hUVECs^{RED}$: $hUVECs^{GFP}$, and $hUVECs^{RED}$: $hUVECs^{HtrA3;\ GFP}$, indicating that $hUVECs^{HtrA3;\ GFP}$ (white arrows) contributed more to the tip position (Scale bar: 200 µm). H) Schematic drawing of the in vitro EC spheroid spouting assay. I) Quantitative analysis of tip cell contribution in the two groups revealed that HtrA3 enhanced specification of hUVECs to become tip cells. (*$p < 0.05$).

Supporting Information). These data thus showed that the HtrA3 enhanced tip cell formation by suppressing the Notch signaling pathway.

Activation of PI3K/AKT plays an essential role in the regulation of Notch signaling. We therefore investigated whether PI3K/Akt is involved in the suppression of DLL4/Notch signaling by HtrA3. We found that the expression levels of PI3K, phosphorylated AKT (phospho S473, p-AKT), and phosphorylated mTOR (phospho S2481, p-mTOR) were upregulated in HtrA3-overexpressing hUVECs, while they were downregulated in HtrA3-knockdown hUVECs (Figure S8G, Supporting Information). Inhibition of PI3K/mTOR signaling with PI-103 significantly promoted NICD protein accumulation in the nuclei (Figure S9, Supporting Information) and increased mRNA levels of Notch target genes (Figure 4F) in the HtrA3-overexpressing group. Moreover, PI-103 nearly completely inhibited tip cell maker expression (Figure 4G) and sprouting in HtrA3-overexpressing hUVECs spheroids (Figure 4H,I);

© 2021 Wiley-VCH GmbH

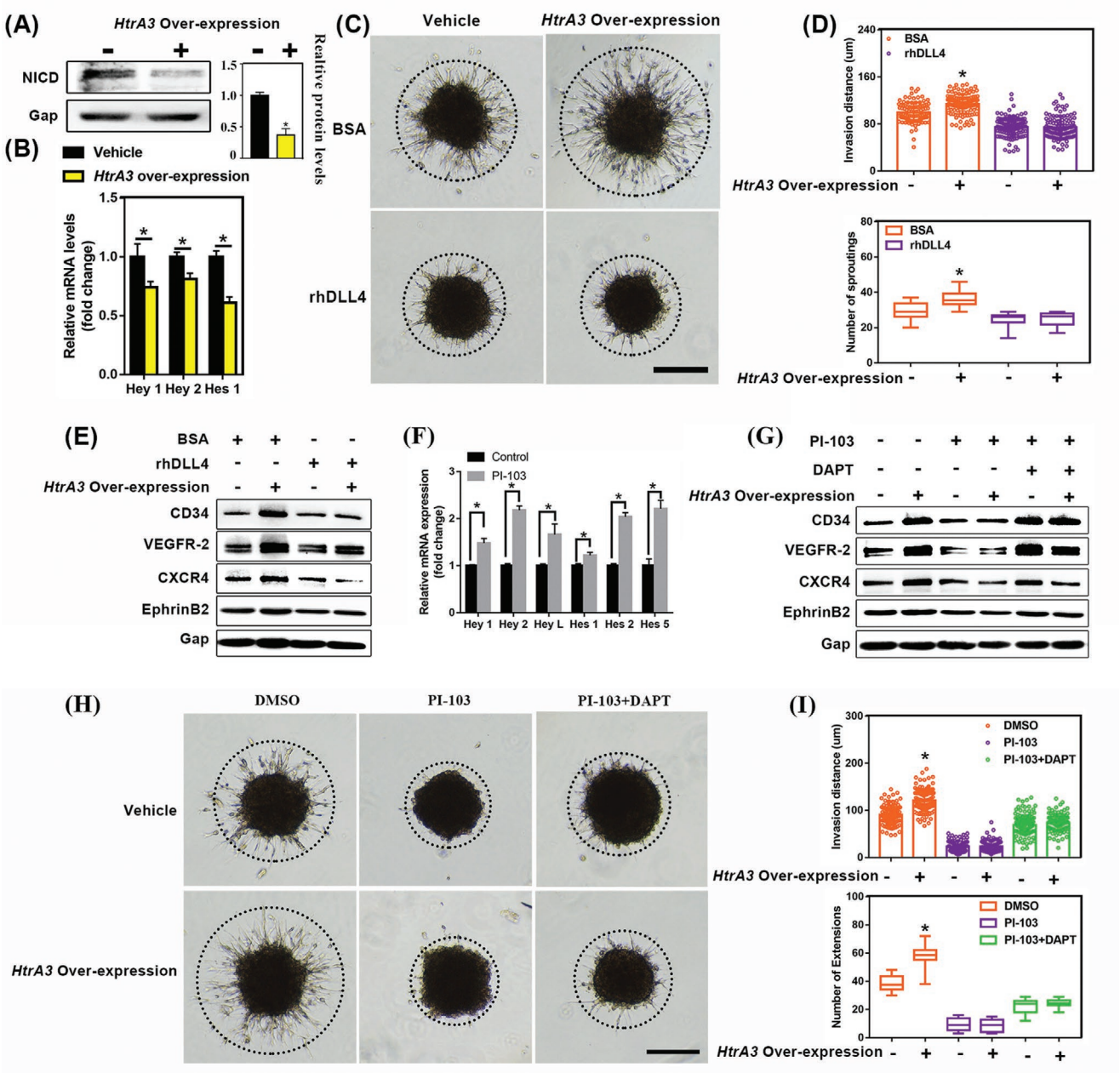

Figure 4. HtrA3 promoted tip cell formation via the PI3K-AKT-Notch signaling pathway. HtrA3 overexpression downregulated A) NICD levels and the B) mRNA expression of Notch target genes. Activation of Notch signaling with rhDLL4 suppressed HtrA3-induced angiogenesis in hUVECs (C) (Scale bar: 200 µm) and the expression of tip cell markers (E), particularly in the HtrA3 over-expression group. D) Quantification analysis of invasion distance and the number of sprouts showed that there were no statistical differences between the HtrA3 over-expression group and control group after rhDLL4 application. Inhibition of the PI3K/AKT/mTOR pathway by PI-103 led to F) enhanced Notch target genes in hUVECs over-expressing HtrA3, G) the decreased expression of HtrA3-induced tip cell markers and H) suppression of HtrA3-induced angiogenesis in hUVECs, which were partly restored by inhibition of Notch signaling with DAPT(Scale bar: 200 µm). I) Quantification analysis of invasion distance and the number of sprouts showed that there were no statistically significant differences between the HtrA3 over-expression group and control group after PI-103 and DAPT application. (*$p < 0.05$).

whereas DAPT largely rescued expression of tip cell makers and angiogenic sprouting in HtrA3-knockdown hUVECs (Figure 4H,I). These data showed that PI3K/AKT/mTOR signaling is involved in suppressing downstream Notch signaling and in promoting tip cell formation in HtrA3-overexpressing hUVECs. PI3K-regulated kinase SGK can enhance degradation of NICD,[16] while active Akt can downregulate NICD transcriptional activity by phosphorylating NICD and inhibiting it's nuclear localization.[17] Therefore, we can deduce that HtrA3 promotes tip cell formation via PI3K/AKT/mTOR-Notch signaling.

PI3K/AKT/mTOR signaling often acts downstream of out-in signal transduction from the ECM. HtrA3 is a secreted serine protease targeting extracellular components during various

© 2021 Wiley-VCH GmbH

physiological and pathological process. We speculated that the signal triggered by secreted HtrA3 is transmitted through the transmembrane structure, most likely involving the integrin family, leading to activation of intracellular PI3K/AKT/mTOR signaling. We focused on integrin β1 (Itgβ1) due to its high expression level in tip cells.[14c] We observed Itgβ1 clustering on the tip positions of sprouts from hUVEC spheroids (**Figure 5**A). Itgβ1 clustering increased in HtrA3-overexpressing hUVECs (Figure 5B), while in HtrA3-knockdown hUVECs, Itgβ1 was apparently downregulated (Figure S10A, Supporting Information). We next found that Itgβ1 blocking with β1 antibody reduced cellular cortical protrusions and increased sphericity in HtrA3-overexpressing hUVECs (Figure S10B,C, Supporting Information). Itgβ1 blocking downregulated PI3K, p-AKT (S473), AKT, p-mTOR (S2481), and mTOR (Figure S10D, Supporting Information) and significantly increased mRNA levels of Notch target genes including Hey1, Hey2, HeyL and Hes1 in HtrA3-overexpressing hUVECs (Figure S10E, Supporting Information). Moreover, Itgβ1 blocking completely eradicated tip cell maker expression (Figure 5C) and increased sprouting in HtrA3-overexpressing hUVECs spheroids (Figure 5D,E, Supporting Information). The reduction in angiogenic sprouting and expression of tip cell makers in HtrA3-overexpressing hUVECs upon Itgβ1 blocking was largely reversed by DAPT-induced Notch pathway inhibition (Figure 5D,E, Supporting Information). Taken together, these results indicate that the effects of HtrA3 on tip cell formation are, in large part, ascribed to regulation of the Itgβ1-PI3K/Akt/mTOR-Notch signaling axis.

2.6. HtrA3 Degrades Collagen IV and Exposes Itgβ1-Related Ligands

We next explored why Itgβ1 is activated by secreted HtrA3. Collagen IV is the main component of vascular basement membrane (BM) surrounding ECs. We hypothesized that HtrA3 secreted from ECs degrades surrounding collagen IV and exposes enwrapped Itgβ1-related ligands. Collagen IV degradation provided space for tip cell morphogenesis. The exposed ligands activated Itgβ1 and initiated the process of outside-in signal transduction.

To prove our hypothesis, we transfected hUVECs with lentivirus encoding HtrA3 recombinant fusion protein and performed spheroid sprouting assay within DQ-collagen IV. DQ-collagen IV is normally free of fluorescence. Once it is degraded, green fluorescence could be detected under confocal microscopy. We found that after 24h culture, red fluorescent HtrA3 fusion protein was observed to co-localize with green fluorescent collagen IV in the sprouting area from hUVECs spheroid, particularly at the tip position of sprouts (Figure 5F), indicating the direct degradation of collagen IV by HtrA3 at the tip position. By contrast, sparse green fluorescence was detected surrounding the untransfected spheroids (Figure S10F, Supporting Information), indicating limited collagen IV degradation ability of untransfected cells compared with HtrA3 fusion protein overexpressing ECs. Western blot analysis showed that there was a decrease in grayscale pixel values after co-incubation of HtrA3 and collagen IV, further confirming enzymatic degradation of collagen IV by HtrA3 (Figure 5G). After addition of recombinant Itgβ1, we observed an apparent increase of Itgβ1 absorption to the HtrA3 digested Matrigel (Figure 5H,I), thus demonstrating that increased ligand exposure led to adsorption of more Itgβ1 to the HtrA3 treated matrices. Triple-helical collagen IV forms a 3D network by combining their C- and N- termini, which is the structural basis of BM and ECM surrounding ECs.[18] Hence, breakdown of collagen IV means reducing barrier for ECs to invade into the surrounding tissue, contributing to cortical protrusion, motility, and angiogenic sprouting. Therefore, exposure of Itgβ1-related ligands in HtrA3 treated matrices can induce outside-in signal transduction, ultimately enhancing tip cell formation through the PI3K/Akt/mTOR signaling and Notch pathway.

2.7. VEGF-VEGFR2 Signaling Regulates HtrA3 Expression

We next explored how HtrA3 expression was regulated in an angiogenic environment. We found that upon VEGF stimulation, mRNA transcripts, protein expression levels of HtrA3 and CD34 in HUVECs increased (Figure S11A,B, Supporting Information). Both increased HtrA3 and CD34 expression levels induced by VEGF were abolished by treatment with SU1498 and SU5416, which are selective VEGFR2 inhibitors (Figure S11C, Supporting Information). Similarly, administration of exogenous VEGF could increase HtrA3 expression in the frontal areas of skin wound healing in mice, while SU5416 application eliminated this phenomenon (Figure S11D, Supporting Information). Moreover, supplementation of rhHtrA3 reversed the inhibitory effects of SU5416 on VEGF-induced CD34 expression by HUVECs (Figure S11E, Supporting Information). VEGF induced increase in the number and length of sprouts on HUVECs spheroids, and these phenomena were abrogated upon treatment with SU5416 (Figure S11F,G, Supporting Information). rhHtrA3 could rescue the inhibitory phenotype by SU5416, increasing invasion distance and number of sprouts from HUVECs spheroids (Figure S11F,G, Supporting Information). Collectively, our data showed that VEGF increases HtrA3 expression through VEGFR2 activation and HtrA3 is implicated, at least partially, in VEGF-elicited tip cell formation and angiogenic response.

2.8. HtrA3 Increases Angiogenesis in Bone Defect Area, while HtrA3 siRNA Decreases Developmental Retinal Angiogenesis

We finally investigated the possibility of utilizing HtrA3 protein and HtrA3 siRNA as therapeutic agents to regulate angiogenesis under pathological situations. To investigate the possibility of using HtrA3 as a therapeutic agent to enhance angiogenesis, we created cranial defects in rats and then administrated exogenous rhHtrA3 (**Figure 6**A). Osmotic pumps were used to slowly release rhHtrA3 into freshly made rat cranial defects for 3 days (Figure S12, Supporting Information). One week later, we observed that rhHtrA3 significantly promoted macroscopic angiogenesis in the defect area (Figure 6C). With immunofluorescence staining, three times more ECs were observed in the defect area of the rhHtrA3 versus control groups (Figure 6D,E).

© 2021 Wiley-VCH GmbH

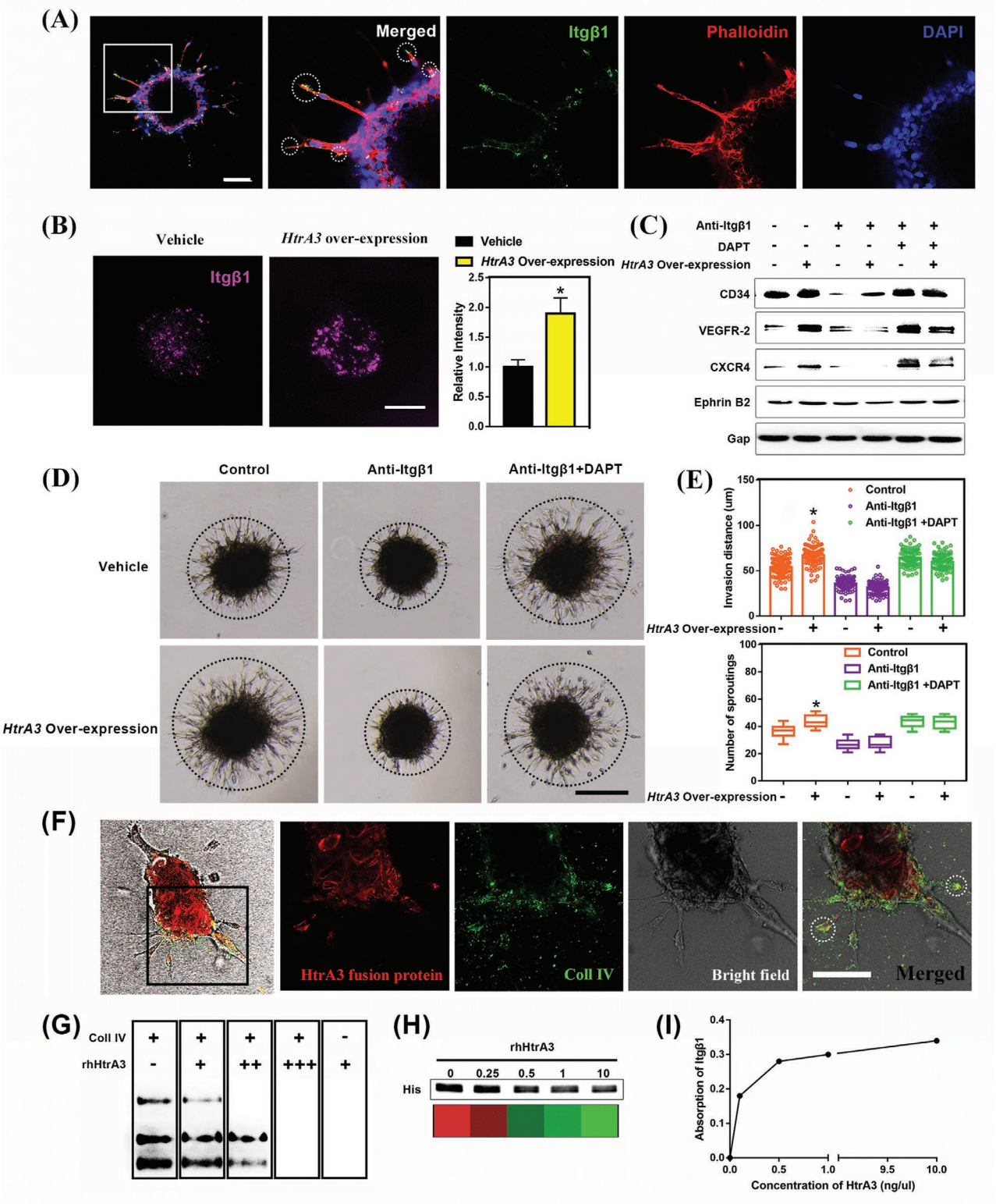

Figure 5. HtrA3 degraded collagen IV, exposing integrin β1 receptor-related ligands in ECM and eventually activating integrin β1, which linked extracellular HtrA3 action and intracellular Notch signaling regulation. A) Integrin β1 clustering was observed on the tip positions of sprouts from hUVEC spheroids (Scale bar: 200 µm). B) Significant clustering of Integrin β1 were found on hUVECs overexpressing HtrA3, which were cultured in matrigel, as compared to the control group. (Scale bar: 10 µm) Inhibition of integrin β1 with β1 antibody C) reduced HtrA3-induced tip cell markers and D) sprouting angiogenesis, which were restored by Notch signaling inhibition by DAPT. E) Quantification analysis of invasion distance and the number of sprouts. F) Co-localization of HtrA3 fusion protein of hUVEC spheroids and degraded green fluorescent collagen IV (Scale bar: 50 µm). G) Western blot analysis of collagen IV – HtrA3 co-culture showed the degradation of collagen IV by rhHtrA3. H,I) Itgβ1 absorption assay showed that more Itgβ1 were dose-dependently adsorbed by the rhHtrA3 degraded matrix. (*$p < 0.05$).

© 2021 Wiley-VCH GmbH

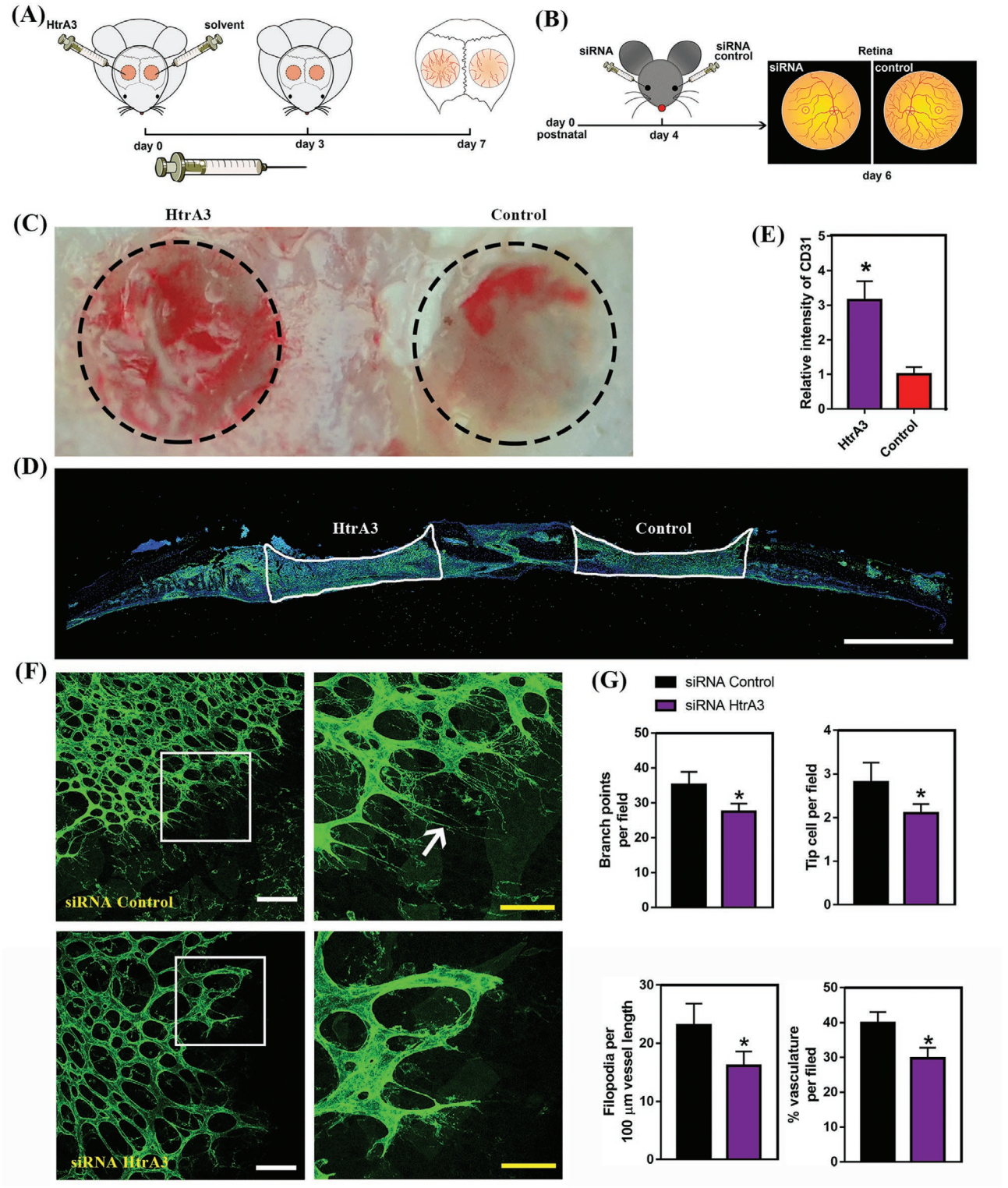

Figure 6. HtrA3 increased angiogenesis in the bone defect area and HtrA3 siRNA decreased retinal sprouting angiogenesis. A) Scheme of HtrA3 application in bone defect area. B) Scheme of HtrA3 siRNA injection in mice. C) Representative images showing that macroscopic angiogenesis was achieved after HtrA3 treatment. D) Immunofluorescence showed more ECs were induced within the defect area, particularly at the edge of the defect. E) Quantification analysis showed the intensity of CD31 immunofluorescence staining in the defect area after HtrA3 administration was threefold as that in the control group. F) Isolectin B4 staining of the developing retinal vessels treated by siRNA control or siRNA HtrA3 at P6 showed that siRNA HtrA3 treatment led to impaired retinal development with tip cell abnormalities. White arrow marked the filopodia of tip cells (White scale bar: 100 μm, yellow scale bar: 50 μm). G) Decreased branch points, tip cells, filopodia, and vasculature were observed after siRNA HtrA3 treatment. (*$p < 0.05$).

 © 2021 Wiley-VCH GmbH

To study the effects of HtrA3 siRNA on developmental retinal angiogenesis, we injected HtrA3 siRNA (0.5 μg) directly into the eyes of 4 days post-natal P4 C57BL/6N mice (Figure 6B). The eyes were harvested 2 days later. We found that HtrA3 siRNA markedly inhibited retinal angiogenesis (Figure 6F), resulting in 20% less tip cells, and 30% less filopodia extensions at the vascular front, 23% less branchpoints within the vascular plexus, and 25% decrease in the area covered by blood vessels, thus indicating severe patterning defects in retinal vessels (Figure 6G). Taken together, these results confirmed that exogenous rhHtrA3 promotes angiogenesis in the bone defect area, while HtrA3 siRNA decreases developmental retinal angiogenesis.

Angiogenesis is a complex, multi-step, and highly coordinated process of new blood vessel formation from pre-existing blood vessels. The formation and characteristics of tip cells account for the morphology and function of the new blood vessels. Many factors, such as DLL4,[6] microRNA-30 (miR-30),[19] activin receptor-like kinase 1 (ALK1),[20] transcription factor NF-E2–related factor 2 (Nrf2),[5] and SRY-related HMG box 17 (SOX17),[21] have been reported to be tip cell regulators. However, they are all intracellular signaling molecules. The crosstalk between ECs and ECM could play key roles in regulating how tip cells anchor on ECM and infiltrate through the surrounding matrix, particularly during the initial stages of angiogenesis. Here, our study shed some light on this process. Specifically, as shown in **Figure 7**, the VEGF concentration exhibits gradient change with increasing distance from hypoxic tissues.[3] ECs closer to the hypoxic area would sense higher concentrations of VEGF and subsequently secrete more HtrA3 to breakdown collagen IV, which is the major component of BM and ECM surrounding ECs. Consequently, the physical barrier against ECs is broken through and Itgβ1-related ligands wrapped in ECM are exposed. Then Itgβ1 is activated through Itgβ1-ligand binding. Subsequently, the Itgβ1-PI3K/AKT/mTOR signaling cascade is activated and the Notch pathway is inhibited, which eventually leads to tip cell specification, resulting in increased cellular cortical protrusion, mobility of ECs, and angiogenic sprouting. Therefore, we can conclude that HtrA3 couples VEGF to regulate tip cell selection. ECs closer to the higher concentration of VEGF secrete more HtrA3, which results in more competitive advantage for tip cell formation. Promoting tip cell formation can enhance angiogenesis which would facilitate tissue repair. Since HtrA3 knockdown contributes to less tip cell specification and impaired vascular remodeling, HtrA3 might be an alternative therapeutic target for diverse diseases characterized by pathological excess angiogenesis, such as cancer, as well as some skin, joint or ocular disorders. To this end, more investigations are needed in the future.

Angiogenesis plays an important role for pathological processes like tumor growth, wound healing and neovascularization of ischemic tissue. Conventionally, several proangiogenic cytokines, such as VEGF and bFGF, have frequently been used to enhance angiogenesis in ischemic area.[22] However, angiogenic therapy with conventional angiogenic proteins (VEGF, bFGF) is associated with several limitations including pathological angiogenesis, fibrosis, and thrombosis due to the nonspecificity.[23] Similarly, since VEGF and its receptors have physiological functions in the normal ECs, blocking VEGF pathway interferes with these functions. Therefore, anti-VEGF drugs for treating diseases characterized by pathological angiogenesis, such as ocular disorder, have also met with argument.[24] Ideally, agents that primarily target tip cells might be more feasible for their limited effects on quiescent ECs.[25] In this study, we found HtrA3 was upregulated in tip cells and promoted tip cell formation. Moreover, significant macroscopic revascularizations in defect area are induced by rHtrA3 administration, indicating its good prospect in therapeutic angiogenesis and neovascularization. Similarly, since HtrA3 knockdown contributes to less tip cell specification and impaired vascular

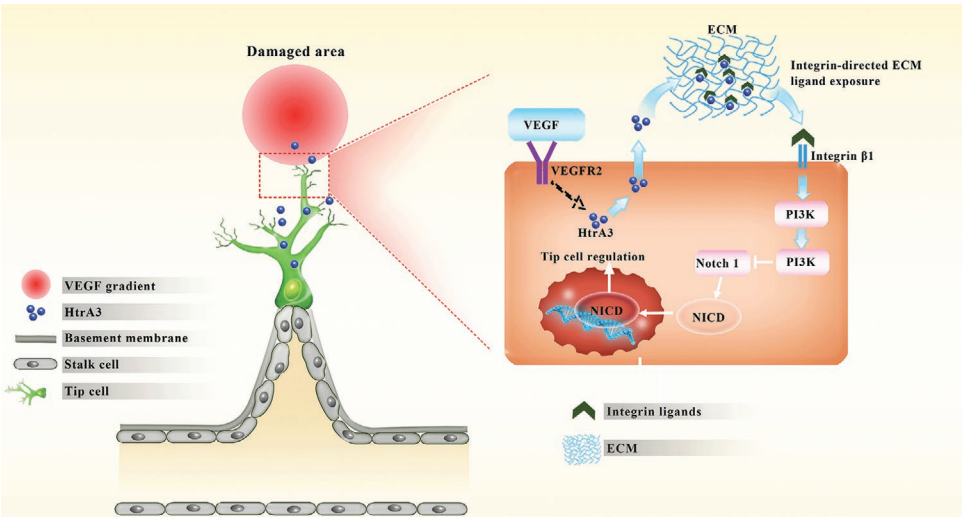

Figure 7. HtrA3 links VEGF to the selection of tip cells. ECs closer to the hypoxic area sense a higher concentration of VEGF and subsequently secrete more HtrA3 to breakdown collagen IV, which is the major component of basement membrane and ECM surrounding ECs. Consequently, the physical barrier against ECs is broken through and Itgβ1-related ligands wrapped in ECM are exposed. Subsequently, Itgβ1 is activated through Itgβ1-ligand binding, which in turn triggers the Itgβ1-PI3K/AKT/mTOR signaling cascade that results in inhibition of the Notch pathway, which eventually enhances tip specification of ECs.

© 2021 Wiley-VCH GmbH

remodeling, anti-HtrA3 might be an alternative therapy for diverse diseases characterized by pathological angiogenesis, such as cancer and skin, joint or ocular disorders. To this end, more investigations are needed.

In summary, our work provides deep insight of how crosstalk between ECs and ECM enhances tip cell formation and angiogenesis in response to angiogenic stimulators such as VEGF. HtrA3 can potentially be a therapeutic molecule for enhancing angiogenesis in tissue repair and tissue engineering, as well as serve as a therapeutic target for the treatment of neoplastic diseases.

3. Experimental Section

Animals and Surgical Procedures: All animal surgical procedures were approved by the Institutional Animal Care and Use Committee of Peking University (No. LA2019297 and LA2018245). To avoid skewing of experimental data by gender and estrus cycle,[26] only male animals were used in this study. 18 male Sprague-Dawley (SD) rats (8 weeks old), 24 male C57BL mice (8 weeks old) and 30 male BALB/c nude mice (4 weeks old) were purchased from the Beijing HFK Bioscience Co. Ltd. (Beijing, China).

For establishing the mandible defect model, the rats (n = 6 in each group) were intraperitoneally anesthetized with phenobarbitol sodium (100 mg per kg); the buccal skin and masseter were then horizontally incised without severing the facial nerves. The posterior border of the mandible was then exposed. A trephine (MR.229.205.040, Meissen, Germany) was used to carefully remove a 3mm core of bone on both sides of the mandibles. Bone debris was washed with sterile saline. The muscle incision was closed with 5–0 resorbable suture (J433H, Vicryl, Ethicon Inc., San Angello, Texas, USA) and the skin was sewn with a 3-0 suture (Jinhuan, Shanghai, China). The mandibula were then harvested for histological analysis immediately (day 0) and on the 3rd and the 7th day after surgery.

To establish the skin defect model, the mice (n = 6 in each group) were anaesthetized by phenobarbitol sodium and a round full-thickness excisional wound was created on the rat dorsum by using iris scissors under sterile surgical conditions. The wound was covered by a single transparent semi-permeable dressing and firmly secured using a surgical adhesive. Samples were harvested for histological analysis on the 4th day after surgery.

Nude mice (n = 6 in each group) were injected subcutaneously with 10^7 hUVECs mixed with 0.1 mL Matrigel at 4 °C on ice. Implants were harvested after 4 days.

To explore the effects of HtrA3 on angiogenesis in the defect area, calvarial defect model was created. Briefly, the rats (n = 6 in each group) were intraperitoneally anesthetized with phenobarbitol sodium (100 mg per kg), and the dorsal cranium was then exposed. Subsequently, full thickness bone defects with a diameter of 3 mm were made in each rat at the center of each parietal bone, using a saline-cooled trephine drill. Defects were flushed with saline to remove bone debris. Osmotic pumps were used to slow the release of 4 µg rHtrA3 at a speed of 1 µL h^{-1} for 3 days into freshly-formed rat cranial defects. Solvent provided by the manufacturer were used as a control. After one week, the whole calvarias were harvested for histological analysis.

To investigate the effects of HtrA3 on retinal vessel formation in vivo, 0.5 µg of HtrA3 siRNA was injected intravitreally into one eye of a P4 neonatal C57BL/6N mouse and control siRNA was injected into the other eye. The eyeball was harvested 2 days later. Flat mounted, fixed tissues were stained with FITC-conjugated isolectin B4 and imaged using a confocal laser scanning microscopy. Then vasculature percentage, branch points, tip cell numbers, and filopodia were quantified as previously described using Image J.

Patients and Tissue Samples: All clinical samples were obtained from patients (n = 3) with oral squamous cell carcinoma (OSCC) who had undergone surgical excision at the Department of Maxillofacial Surgery, Oral Hospital of Peking University (Beijing, China). All study protocols were reviewed and approved by the Institutional Animal Care and Use Committee of Peking University. Informed consent was obtained from all patients in accordance with institutional guidelines.

Fluorescent Immunohistochemistry: Tissue processing and sectioning were carried out as previously described.[27] Briefly, tissue samples were fixed in 10% (w/v) neutral buffered formalin for 7 days, decalcified (for bone tissues only), and dehydrated according to standard protocols. Next, samples were embedded in paraffin and 5 mm thick sections were prepared. Then the sections were deparaffinized and rehydrated, and antigen retrieval was performed in a microwave oven (800 W for 20 min) with citrate buffer. The slides were then washed with PBS three times for 5 min each. The sections were blocked with 5% (w/v) bovine serum albumin (BSA) in phosphate-buffered saline (PBS) for 30 min at room temperature, and then incubated with the primary antibodies anti-CD34 (ab81289; Abcam) and anti-HtrA3 diluted in 1% (w/v) BSA overnight at 4 °C. Then, the slides were washed three times by PBS and probed with the secondary antibodies, Alexa Fluor-488 and Fluor-563 (ab150075; Abcam), for 1 h at room temperature. The nuclei were stained by DAPI. The cells were washed three times by PBS before fixation using Fluoromount-G (00-4958-02; Thermo Fisher cientific, Rockford, IL, USA). The coverslips were finally sealed using nail polish. Pictures were captured under confocal microscopy.

Cell Culture: Human primary cell lines, hUVECs, were purchased from ScienCell Research Laboratories and cultured in endothelial cell medium (ECM; 1001; ScienCell Research Laboratories), within a humidified chamber with 5% CO_2 at 37 °C.

Lentiviral Vector Production and Transfection: All lentiviral vectors encoding green fluorescent protein (GFP) for knockdown of HtrA3 were purchased from GeneChem Co., Ltd. (Suzhou, China).

Sequence of shRNA #1: 50-CCGGCGACAACAAGTCCCTTTGTAACTCGAGTTACAAAGGGACTTGTTGTCGTTTTTG-3′.

Sequence of shRNA #2: 50-CCGGCTGGTACTATACCCACAGATACTCGAGTATCTGTGGGTATAGTACCAGTTTTTG-3′.

Cells transfected with scramble were utilized as controls.

The lentiviral vector encoding GFP and the HtrA3 gene to upregulate HtrA3 was also purchased from GeneChem Co., Ltd. (Shanghai, China). The lentiviral vector with HtrA3 fusion protein (fused to mCherry) was also purchased.

One day before lentiviral transfection, hUVECs were seeded in six-well plates at a density of 3×10^5 cells per well. Next, lentiviral vectors overexpressing HtrA3 or shRNA were added with 5 mg mL^{-1} polybrene (GeneChem) to the cell culture for 12 h. Then the transfected cells were selected using puromycin (P8833; Sigma–Aldrich) for 3 days.

Western Blot: Western blot was performed as previously described.[28] The following antibodies were used: anti-GAPDH (ab9485; Abcam), anti-HtrA3 (A14649, ABclonal), anti-CD34 (ab81289, Abcam), anti-VEGFR2 (ab39256, Abcam), anti-CXCR4 (ab181020, Abcam), anti-Ephrin B2 (ab150411; Abcam), anti-Notch1 (ab52627, Abcam), anti-PI3K (ab86714; Abcam), anti-AKT phospho S473 (4060; Cell Signaling Technology, Boston, MA, USA), anti-AKT (4691; Cell Signaling Technology), anti-mTOR (ab32028; Abcam), anti-mTOR phospho S2481 (ab137133; Abcam), anti-integrin β1 (ab183666, Abcam), and anti-Notch-intracellular domain (NICD) (ab8925, Abcam). The secondary antibody was HRP-labeled IgG (A0208, A0216; Beyotime).

RT-qPCR Analysis: Reverse transcription was achieved using a PCR thermal cycler (Takara). Optical 96-well reaction plates (Thermo Fisher Scientific) and optical adhesive films (Thermo Fisher Scientific) were used for PCR. Data were analyzed using QuantStudio Design & Analysis Desktop Software (Thermo Fisher Scientific). Differences in gene expression levels among different groups were statistically analyzed. The primer sequences are shown in Table S1. GAPDH served as the internal control.

© 2021 Wiley-VCH GmbH

In Vitro Tube Formation Assay: 24-well plates were coated with 250 µL Matrigel (Becton, Dickinson and Company, Franklin Lakes, NJ, USA) per well without introducing air bubbles. Then, the plates were put in an incubator for at least 30 min to allow the Matrigel to gel. Next, hUVECs ($1*10^5$ in 0.5 mL per well) transfected by different lentiviral vectors were plated on the Matrigel. Finally, the 24-well plates were incubated at 37 °C in 5% CO_2 air incubator. Tube structures were observed under confocal microscopy after 4 h. Relative total tubule length, sum of the number of junctions, and tubules in five different fields were quantified using Image Pro Plus software to assess tube formation.

Wound Healing Assay: HUVECs of different treatment groups were seeded onto 6-well plates. When the cells formed a confluent monolayer, scratches were made with a 1 mL pipette tip. The scratched monolayers were washed with PBS to remove floating cells and debris. Subsequently, 1 mL of BD Matrigel TM (4.5 mg mL^{-1}) were added into the cells and were allowed to polymerize for 0.5 h, prior to adding serum-free medium on the top of the set Matrigel. The ability of hUVECs to close the wounded space was used to assess their migration ability. Cell migration into the wound was assessed by microscopy using a digital inverted microscope after 24 h. The area covered by migrating cells in the initial wound was measured using Image Pro Plus software.

Transwell Cell Invasion Assay: HUVECs cell invasion assay was performed using transwell cell culture inserts (Transwell Assay System; Corning, High Wyombe, UK) for 24-well plates. Before starting the assay, the upper polycarbonate membrane was coated with diluted Matrigel. Then, two hundred microliters (1×10^5 cells per mL) of serum-starved hUVECs were added to the upper polycarbonate membrane chambers (pore size, 8 µm) and incubated at 37 °C. The lower chambers contained cultured medium with 10% (v/v) fetal bovine serum. After 24 h of incubation, the cells, which had not crossed the membrane were removed with a wet cotton and then the undersides of the filters were fixed with 4% (w/v) paraformaldehyde for 10 min at room temperature and then stained with 0.5% crystal violet for 10 min. The number of migratory cells was counted five times within random fields of the microscope. Experiments were performed in triplicates and images of the cells, which had migrated to the underside of the inserts were captured.

Generation of Endothelial Cell Spheroids: Agarose (2% w/v) was used to form molds for endothelial cell spheroids, whilst preventing adhesion of cells to the mold surface. The agarose (2% w/v) was heated to form a melted solution and added into a 3D Petri Dish (Microtissues). After solidification, the agrose moulds were placed in a six-well plate for culturing cells. Then, 200 µL of cell suspension was seeded on each mold. Fifteen minutes later, the culture medium was added and cellular aggregates were allowed to form for 24 h.

In the mosaic EC spheroid assay, either $hUVECs^{GFP}$ or $hUVECs^{HtrA3}$; GFP were respectively mixed at a 1 : 1 ratio with $hUVECs^{RED}$ to generate EC mosaic spheroids.

The Spheroid-Based Angiogenesis Model: For the in vitro sprouting angiogenesis assay, spheroids were generated overnight, after which they were embedded into 2.5% (w/v) gelatin methacryloyl gels, with or without HtrA3 (25 ng mL^{-1}, R&D Systems). After light curing, culture medium was added. The spheroids were allowed to sprout for 12 h. Then, in vitro sprouting was quantitated digitally by measuring the number of extensions and the length of the sprouts (calculated as cellular invasion distance) that had grown out of each spheroid using the Image Pro Plus software, and analyzing ten spheroids per experimental group and experiment.

For the mosaic spheroid sprouting angiogenesis assay, a collagen stock solution (equilibrated to 2 mg mL^{-1}, pH = 7.4) was prepared prior to use by mixing: acidic collagen extract of rat tails, 10 × PBS, distilled water and 1 mol L^{-1} NaOH, according to instructions of the manufacturer. This stock solution was mixed at a 1 : 2 ratio with a mixture of Matrigel and ECM basal medium (1 : 1) containing 20% (v/v) FBS (Biochrom, Berlin, Germany) and 0.5% (w/v) methylcellulose, to prevent sedimentation of spheroids prior to polymerization of the collagen gel. The spheroids were allowed to sprout for 24 h.

Proliferation Assay: Both EdU (ethynyl-deoxyuridine) cell proliferation assay and real-time observations were performed to assay the proliferation of hUVECs. hUVECs were cultured in culture medium with EdU for 2h before being fixed.

Immunostaining of Cell Cultures: For immunofluorescence microscopy, cell suspensions were obtained by pancreatin treatment of adherent endothelial cell monolayers. Cells were fixed for 15 min with freshly-prepared 2% (w/v) paraformaldehyde in PBS, permeabilized for 10 min in 0.1% (v/v) Triton X-100, blocked for 1 h in 5% (w/v) BSA at room temperature and incubated overnight at 4 °C with the primary antibodies. Then, the cells were washed three times with phosphate-buffered saline (PBS) and labeled with the secondary antibodies, Alexa Fluor-647 (ab150075; Abcam), for 1 h at room temperature. The nuclei were stained with DAPI. The cells were washed three times by PBS before fixation using Fluoromount-G (00-4958-02; Thermo Fisher cientific, Rockford, IL, USA). Pictures were captured under a confocal microscope. The following antibodies were used: anti-HtrA3 (A14649, ABclonal), anti-CD34 (ab81289; Abcam).

Flow Cytometry Analysis: Cell suspensions were obtained by pancreatin treatment of adherent endothelial cell monolayers. All immunofluorescent labeling and washing were performed in PBS containing 0.1% (w/v) BSA. Cells were fixed in 2% (w/v) paraformaldehyde in PBS for 15 min at room temperature and incubated with the primary antibodies anti-CD34 (ab81289; Abcam) diluted in 1% (w/v) BSA. Then, the cells were washed three times with phosphate-buffered saline (PBS) and probed with secondary antibodies, Alexa Fluor-647 (ab150075; Abcam), for 1 h at room temperature. The cell nuclei were stained with DAPI. The cells were then washed three times by PBS, and were analyzed by flow cytometry on a FACSCalibur (Becton Dickinson) in combination with the FlowJo software (Tree Star, San Carlos, CA, USA).

Inhibitors: PI3K/mTOR inhibitor PI-103, VEGFR2 inhibitors, SU1498 and SU5416, were all purchased from Medchemexpress, New Jersey, America.

Live Cell Proteolysis Assay: Live cell proteolysis assay was performed as previously described with minor modification to the protocol.[29] Briefly, EC spheroids were coated with the mixed gel mentioned above, but containing 25 µg mL^{-1} DQ-gelatin and incubated in an incubator for 30 min to solidify. Then, culture medium containing 10% (v/v) FBS was added and the spheroids were allowed to sprout for 24 h. Proteolysis of DQ-collagen IV (green fluorescence) was observed in live cells under confocal microscopy, utilizing 25x water immersion objective lens.

Proteolysis Assay of Collagen IV: 250 ng Collagen IV (ab7536, Abcam) was mixed with rhHtrA3 solution (Abnova, Taiwan, China) containing 0, 250, 400, 800 ng of rhHtrA3, and the mixture was incubated for 12 h. Then the mixture was used for western blot analysis. The rhHtrA3 solution without collagen IV was utilized as the control group.

Detection of β1 Ligand Exposure: 96-well plates were coated with 50 uL of Matrigel (Becton, Dickinson and Company, Franklin Lakes, NJ, USA) and were allowed to polymerize for 0.5 h prior to adding 0, 0.25, 0.5, 1 and 10 µg μL^{-1} of rhHtrA3 diluted in solvent provided by Abnova (Taiwan, China) on the top of the set Matrigel (50 µL per well). Subsequently, the plates were incubated for 12 h at 37 °C and then the liquid was removed. The wells were washed three times with PBS prior to adding 30 µL of 1 ug mL of recombinant human $\alpha v\beta 1$ protein (ab246162, Abcam) labeled with his. After culturing for 2 h at 37 °C, 20 uL from each well was used for western blot. Anti-his antibody was used as the primary antibody.

Statistical Analysis: Results were expressed as mean ± SEM. Analysis between two paired samples was performed using a two-tailed unpaired Student's *t* test. Analysis between more than two sample groups was performed using a one-way unstacked ANOVA. *P* values less than 0.05 were considered statistically significant.

Supporting Information

Supporting Information is available from the Wiley Online Library or from the author.

 © 2021 Wiley-VCH GmbH

Acknowledgements

Y.G., S.M., and M.X. contributed equally to this work. This work was supported by the National Key R&D Program of China (2018YFC1105303/04), National Natural Science Foundation of China (Nos. 81991505, 82022016, 51772006, 31670993, 51973004) and Beijing Municipal Science & Technology Commission Projects (Z181100002018001).

Conflict of Interest

The authors declare no conflict of interest.

Data Availability Statement

Research data are not shared.

Keywords

angiogenesis, extracellular matrix, filopodia, HtrA3, tip cell

Received: January 20, 2021
Revised: April 14, 2021
Published online: May 24, 2021

[1] a) F. Hillen, A. W. Griffioen, *Cancer Metastasis Rev.* **2007**, *26*, 489; b) P. Carmeliet, *Nature* **2005**, *438*, 932.
[2] S. F. De, I. Segura, B. K. De, P. J. Hohensinner, P. Carmeliet, *Arterioscler., Thromb., Vasc. Biol.* **2009**, *29*, 639.
[3] H. Gerhardt, M. Golding, M. Fruttiger, C. Ruhrberg, A. Lundkvist, A. Abramsson, M. Jeltsch, C. Mitchell, K. Alitalo, D. Shima, C. Betsholtz, *J. Cell Biol.* **2003**, *161*, 1163.
[4] a) J. D. Leslie, L. Ariza-McNaughton, A. L. Bermange, R. McAdow, S. L. Johnson, J. Lewis, *Development* **2007**, *134*, 839; b) Y. Blum, H.-G. Belting, E. Ellertsdottir, L. Herwig, F. Lüders, M. Affolter, *Dev. Biol.* **2008**, *316*, 312.
[5] Y. Wei, J. Gong, R. K. Thimmulappa, B. Kosmider, S. Biswal, E. J. Duh, *Proc. Natl. Acad. Sci. USA* **2013**, *110*, E3910.
[6] a) M. Hellström, L. Phng, J. J. Hofmann, E. Wallgard, L. Coultas, P. Lindblom, J. Alva, N. A. Katrin, L. Karlsson, N. Gaiano, K. Yoon, J. Rossant, M. L. Iruela-Arispe, M. Kalén, H. Gerhardt, C. Betsholtz, *Nature* **2007**, *445*, 776; b) I. B. Lobov, R. A. Renard, N. Papadopoulos, N. W. Gale, G. Thurston, G. D. Yancopoulos, S. J. Wiegand, *Proc. Natl. Acad. Sci. USA* **2007**, *104*, 3219.
[7] a) S. E. M. Boas, R. M. H. Merks, *BMC Syst. Biol.* **2015**, *9*, 86; b) B. Cruys, B. W. Wong, A. Kuchnio, D. Verdegem, A. R. Cantelmo, L. C. Conradi, S. Vandekeere, A. Bouché, I. Cornelissen, S. Vinckier, *Nat. Commun.* **2016**, *7*, 12240; c) A. Satoshi, N. Koichi, K. Toshiyuki, A. Yuichiro, H. Yuji, S. Kei, K. Hiroaki, U. Yasunobu, K. Yukiko, K. Hiroki, *Development* **2011**, *138*, 4763.
[8] a) J. Xu, D. Rodriguez, E. Petitclerc, J. J. Kim, M. Hangai, *J. Cell Biol.* **2001**, *154*, 1069; b) X. Xu, Z. Chen, Y. Wang, Y. Yamada, B. Steffensen, *Biochem. J.* **2005**, *392*, 127.
[9] a) S. J. Atkinson, M. L. Patterson, M. J. Butler, G. Murphy, *FEBS Lett.* **2001**, *491*, 222; b) I. Yana, H. Sagara, S. Takaki, K. Takatsu, K. Nakamura, K. Nakao, M. Katsuki, S.-i. Taniguchi, T. Aoki, H. Sato, S. J. Weiss, M. Seiki, *J. Cell Sci.* **2007**, *120*, 1607.
[10] a) R. Timpl, J. C. Brown, *BioEssays* **1996**, *18*, 123; b) N.-B. Liabakk, I. Talbot, R. A. Smith, K. Wilkinson, F. Balkwill, *Cancer Res.* **1996**, *56*, 190.
[11] N. Gui-Ying, L. Ying, M. Hiroyuki, B. Leigh, G. T. Ooi, J. K. Findlay, L. A. Salamonsen, *Mol. Hum. Reprod.* **2003**, *9*, 279.
[12] a) M. A. Bowden, A. E. Drummond, P. J. Fuller, L. A. Salamonsen, J. K. Findlay, G. Nie, *Mol. Cell. Endocrinol.* **2010**, *327*, 13; b) M. Yujiro, U. Narikazu, M. Takuma, M. Kaoru, M. Ken, T. Ken-Ichiro, M. Chieko, S. Jun, T. Hiroshi, H. Kiyoshi, *Oral Oncol.* **2015**, *51*, 84; c) S. Harmeet, E. Yaeta, N. Guiying, *Hum. Reprod.* **2011**, *26*, 748; d) T. Wenta, D. Zurawa-Janicka, M. Rychlowski, M. Jarzab, P. Glaza, A. Lipinska, K. Bienkowska-Szewczyk, A. Herman-Antosiewicz, J. Skorko-Glonek, B. Lipinska, *J. Proteomics* **2018**, *177*, 88.
[13] M. J. Siemerink, I. Klaassen, I. M. C. Vogels, A. W. Griffioen, C. J. F. V. Noorden, R. O. Schlingemann, *Angiogenesis* **2012**, *15*, 151.
[14] a) S. Suphansa, S. Sascha, C. L. Essmann, G. A. Wilkinson, M. E. Pitulescu, A. Till, A. P. Amparo, *Nature* **2010**, *465*, 487; b) G. A. Strasser, J. S. Kaminker, T. L. Marc, *Blood* **2010**, *115*, 5102; c) R. Del Toro, C. Prahst, T. Mathivet, G. Siegfried, J. S. Kaminker, B. Larrivee, C. Breant, A. Duarte, N. Takakura, A. Fukamizu, *Blood* **2010**, *116*, 4025.
[15] a) J. S. Fang, B. G. Coon, N. Gillis, Z. Chen, J. Qiu, T. W. Chittenden, J. M. Burt, M. A. Schwartz, K. K. Hirschi, *Nat. Commun.* **2017**, *8*, 2149; b) X. Zheng, S. Narayanan, V. G. Sunkari, S. Eliasson, I. R. Botusan, J. Grunler, F. Radtke, C. Xu, A. Zhao, N. R. Ekberg, U. Lendahl, S. B. Catrina, *Proc. Natl. Acad. Sci. USA* **2019**, *116*, 6985.
[16] J. S. Mo, E.-J. Ann, J.-H. Yoon, J. Jung, Y.-H. Choi, H.-Y. Kim, J.-S. Ahn, S.-M. Kim, M.-Y. Kim, J.-A. Hong, M.-S. Seo, F. Lang, E.-J. Choi, H.-S. Park, *J. Cell Sci.* **2011**, *124*, 100.
[17] a) J. Song, S. Park, M. Kim, I. Shin, *FEBS Lett.* **2008**, *582*, 1693; b) S. Baek, M. Kim, J. Mo, E. Ann, *Cancer Lett.* **2007**, *255*, 117.
[18] M. E. Than, H. Stefan, H. Robert, R. Albert, M. Karlheinz, K. Klaus, T. Rupert, G. P. Bourenkov, H. D. Bartunik, B. Wolfram, *Proc. Natl. Acad. Sci. USA* **2002**, *99*, 6607.
[19] Q. Jiang, M. Lagos-Quintana, D. Liu, Y. Shi, C. Helker, W. Herzog, F. le Noble, *Hypertension* **2013**, *62*, 592.
[20] B. Larrivée, C. Prahst, E. Gordon, R. del Toro, T. Mathivet, A. Duarte, M. Simons, A. Eichmann, *Dev. Cell* **2012**, *22*, 489.
[21] J. Goveia, A. Zecchin, F. M. Rodriguez, S. Moens, P. Stapor, P. Carmeliet, *Circ. Res.* **2014**, *115*, 205.
[22] C. Kalka, T. Takahashi, H. Masuda, T. Asahara, J. M. Isner, *Med. Klin.* **1999**, *94*, 193.
[23] R. Chitta, A. Patra, B. Kumar, *Nanomedicine* **2013**, *8*, 1735.
[24] a) A. N. Witmer, G. F. J. M. Vrensen, C. J. F. V. Noorden, R. O. Schlingemann, *Prog. Retinal and Eye Res.* **2003**, *22*, 1; b) S. G. Magali, A. S. R. Maharaj, T. E. Walshe, B. A. Tucker, S. Eiichi, K. Tomoki, D. C. Darland, M. J. Young, P. A. D'Amore, C. L. Tailoi, *PLoS One* **2008**, *3*, e3554.
[25] M. J. Siemerink, I. Klaassen, C. J. F. Van Noorden, R. O. Schlingemann, *J. Histochem. Cytochem.* **2013**, *61*, 101.
[26] a) X. Yao, M. S. Carleton, A. D. Kettle, J. Melander, C. L. Phillips, Y. Wang, *Ann. Biomed. Eng.* **2013**, *41*, 1139; b) C. W. Oh, J. Hoover-Plow, E. F. Plow, *J. Thromb. Haemostasis* **2003**, *1*, 1683.
[27] X. Zhang, C. Zhang, Y. Lin, P. Hu, Y. Shen, K. Wang, S. Meng, Y. Chai, X. Dai, X. Liu, X. Mo, C. Cao, S. Li, D. Xuliang, C. Lili, *ACS Nano* **2016**, *10*, 7279.
[28] C. Cao, Y. Huang, Q. Tang, C. Zhang, L. Shi, J. Zhao, L. Hu, Z. Hu, Y. Liu, L. Chen, *Biomaterials* **2018**, *172*, 1.
[29] D. Cavallo-Medved, D. Rudy, G. Blum, M. Bogyo, D. Caglic, B. F. Sloane, *Exp. Cell Res.* **2009**, *315*, 1234.

© 2021 Wiley-VCH GmbH